RSC Advances

ROYAL SOCIETY OF CHEMISTRY

www.rsc.org/advances

RSC Advances

PAPER

Synthesis of γ-Fe_2O_3@SiO_2@Polypyrrole Core/Shell/Shell Nanospheres with Flexible Controllability of Electromagnetic Properties

Received 00th January 20xx,
Accepted 00th January 20xx

DOI: 10.1039/x0xx00000x

www.rsc.org/

Yajie Zhang,[a] Zhiming Zhang,*[a] Shicong Xu,[b] Liangmin Yu,*[a] and Qunwei Tang[c]

A new anchored method by -SO_3H groups was proposed to prepare γ-Fe_2O_3@SiO_2@polypyrrole (γ-Fe_2O_3@SiO_2@PPy) nanospheres with core/shell/shell structure. In the reaction process involved, the sulfonic-functionalized γ-Fe_2O_3@SiO_2 (γ-Fe_2O_3@SiO_2-SO_3H) acts as the core for the polymerization of pyrrole. And PPy can be anchored to form on the surface of γ-Fe_2O_3@SiO_2 to form γ-Fe_2O_3@SiO_2@PPy nanospheres with the help of the sulfonic groups on the surface of γ-Fe_2O_3@SiO_2. Moreover, a flexible controllability of the conductivity and saturation magnetization of the resulting γ-Fe_2O_3@SiO_2@PPy nanospheres can be realized through this method. The resulting electromagnetic γ-Fe_2O_3@SiO_2@PPy nanospheres show maximum conductivity of 53 S cm^{-1} and saturation magnetization of 8.17 Am^2 kg^{-1}. This method reported here may provide us an efficient way to realize the best impedance matching between complex permeability and complex permittivity.

Introduction

Electromagnetically functionalized micro/nanostructures of conducting polymers have triggered growing interests due to their specific applications in electromagnetic interference shielding and microwave absorption.[1,2,3] It has been reported that microwave absorbing properties can be enhanced via the complementation of dielectric loss and magnetic loss. The electromagnetically functionalized composites composed of magnetic nanoparticles (MNPs) and conducting polymers not only have dielectric loss and magnetic loss, but also a synergistic effect of the dielectric loss and magnetic loss.[4,5] So it is very interesting to obtain electromagnetically functionalized conducting polymers. Early study on preparing the electromagnetically functionalized micro/nanostructures of conducting polymers is mainly placed on a two-step method (TSM) including preparation of polyaniline (PANI) nanotubes containing Fe_3O_4 NPs[6] and coaxial PANI/γ-Fe_2O_3 nanofibers[7] by an in-situ chemical oxidation polymerization in the presence of Fe_3O_4 NPs or γ-Fe_2O_3 nanoneedles. A remaining problem on this aspect is the aggregation of MNPs, leading to unhomogeneous distribution in conducting polymer system. By addressing this issue, we have developed a simple chemical one-step method (COSM) in our previous study to prepare PANI/γ-Fe_2O_3 nanofibers.[8] This COSM has successfully realized the one-step synthesis of electromagnetically functionalized composite nanofibers, in which $FeCl_3$ can act as the oxidant for the aniline polymerization reaction and as a source of Fe^{III} for the precipitation of γ-Fe_2O_3 magnets, allowing for a simultaneous preparation of the conducting polymer and magnetic γ-Fe_2O_3 as well as homogeneous distribution of magnetic γ-Fe_2O_3 NPs in the hybrids. More recently, an improved COSM (ICOSM) has also been created to prepare uniform electromagnetic PPy/γ-Fe_2O_3 nanospheres having high electrical conductivity without compromising the magnetic properties.[9] However, it is hard to regulate the electrical conductivity and saturation magnetization independently for this ICOSM.

It is noted that the use of core/shell structure has been an efficient way for improving the microwave absorption properties in recent years.[10,11,12] Especially, the MNPs/conducting polymer core/shell structure has also been reported [1,13]. Moreover, it is possible to control the magnetism and conductivity independently by regulating the dosage of MNPs cores and the polymerization condition of conducting polymer shell, respectively. However, the emulsifiers or/and stabilizers were introduced in order to conducting polymer coated well on the magnetic nanoparticles. The weak interactions between the magnetic nanoparticles and conducting polymers make it hard to ensure the magnetic nanoparticles to be coated well.

It is well known that silica layer formed on the surface of MNPs can screen the magnetic dipolar attraction between MNPs, favoring the dispersion of MNPs in liquid media and protects them from etching in an acidic environment.[14] Furthermore, the silica surface is active to be grafted by specific functional groups such as amidogen,[15,16] sulfonic acid group,[17,18,19] or be modified by chitosan[20] or poly(N-

[a] Key Laboratory of Marine Chemistry Theory and Technology, Ministry of Education, Ocean University of China, Qingdao 266100, China. E-mail: zzmcyj@ouc.edu.cn, yuyan@ouc.edu.cn
[b] College of Physics & Collaborative Innovation Center for Low-Dimensional Nanomaterials and Optoelectronic Devices, Qingdao University, Qingdao 266071, China.
[c] Institute of Materials Science and Engineering, Ocean University of China, Qingdao 266100, China.

vinylpyrrolidone)[21] to anchor the polymerization reaction. Moreover, it is noted that silica is one of the most popular wave-transmitting materials.[22,23] The superior characteristics of silica inspire us to design a sandwiched γ-Fe_2O_3@SiO_2@PPy core/shell/shell structure. In details, the silica-coated γ-Fe_2O_3 (γ-Fe_2O_3@SiO_2) core/shell composite spheres is prepared and then modified with sulfonic acid groups (-SO_3H), which are subsequently employed to guide the oxidation polymerization of pyrrole monomers on the γ-Fe_2O_3@SiO_2 surface. Through this, the γ-Fe_2O_3@SiO_2@PPy core/shell/shell nanospheres were prepared successfully and the weak interfacial interactions between the inorganic γ-Fe_2O_3 MNPs and organic PPy, as well as the poor wave-transmissivity may be improved efficiently at the same time.

Experimental

Materials

The chemicals used in this work, such as $FeCl_3 \cdot 6H_2O$, $FeSO_4 \cdot 7H_2O$, tetraethoxysilane (TEOS), *p*-toluenesulfonic acid (*p*-TSA), 3-mercaptopropyltrimethoxysilane (MPTS) and pyrrole, were all of analytical purity provided by the Shanghai Sinopharm Chemical Reagent Co., and were used as received without further purification. Deionized water was used in all experiments.

Preparation of functional Fe_3O_4 NPs

Fe_3O_4 NPs were prepared by chemical precipitation method according to previous literature.[14] In details: 54.06 g of $FeCl_3 \cdot 6H_2O$ (0.2 mol) and 27.80 g of $FeSO_4 \cdot 7H_2O$ (0.1 mol) were dissolved in 440 mL of deionized water. The obtained transparent solution was degassed with nitrogen flow and then 60 mL of NaOH (16.67 M) was dropped into the above solution within 1 h under vigorous agitation. After reaction at 1 h at 20 °C and subsequent heating at 90 °C for 1 h, the resulting black precipitates were collected and thoroughly rinsed with deionized water and ethanol and dried at 50 °C in vacuum for 12 h.

The as-synthesized Fe_3O_4 NPs were modified by citric acid to get highly dispersed and chemically stable aqueous magnetic fluids (MFs).[24] Briefly, 1 g of Fe_3O_4 NPs and 1.7 g of citric acid were dispersed in 200 mL of deionized water under supersonic agitation for 1 h. The pH value of the reagent was adjusted to 4.8 with hydrochloric acid, and the reaction was allowed to proceed with stirring for 12 h at room temperature. Subsequently, the modified Fe_3O_4 NPs were collected and thoroughly rinsed with deionized water/acetone mixture to remove the residual citric acid, the volume of the mixture was 100 mL and the volume ratio of water to acetone was 1:4. Finally, the modified Fe_3O_4 NPs were dispersed in 100 mL of deionized water for further use.

Preparation of γ-Fe_2O_3@SiO_2 (FS) core/shell nanospheres

20 mL of Fe_3O_4 MFs (10 mg mL^{-1}) was mixed with 80 mL of ethanol and 2.4 mL of 28 wt% aqueous ammonia. After ultrasonic agitation for 1 h, 2 mL of TEOS was added dropwise to the above dispersion and the reaction was proceeded under supersonic stirring for 2 h. The obtained product was collected by magnetic separation and rinsed with concentrated HCl, deionized water and ethanol three times, respectively, and then dried at 50 °C for 4 h. Finally, the γ-Fe_2O_3@SiO_2 nanospheres were heated at 300 °C for 5 h in air. The obtained γ-Fe_2O_3@SiO_2 was designated as FS.

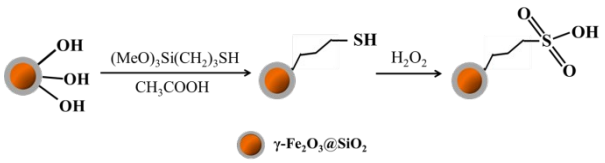

Scheme 1. Schematic illustration for synthesizing sulfonic-functionalization FS nanospheres.

Sulfonic-functionalization of γ-Fe_2O_3@SiO_2 (FSH) core/shell nanospheres

The FS nanospheres were functionalized with -SO_3H according to previous literature[18] and the approach employed was shown in Scheme 1. The FSH nanospheres were achieved by reacting MPTS with the silanol terminal groups to introduce mercapto groups on the surface of silica followed by oxidation with H_2O_2 resulting in covalently bounded –SO_3H groups. Briefly, 1 g of FS nanospheres were dispersed in a mixture containing 30 mL of acetic acid and 4 mL of H_2O_2 (30 wt%) under supersonic agitation. Subsequently, 2 g of MPTS were added and the reaction was allowed to proceed at 80 °C for 3 h. After that, the precipitates were collected by magnetic separation and washed with ethanol three times, and then dried at 50 °C for 12 h. The obtained γ-Fe_2O_3@SiO_2-SO_3H was designated as FSH.

Preparation of γ-Fe_2O_3@SiO_2@PPy (FSHP_x-*y*) core/shell/shell nanospheres

The typical processes for γ-Fe_2O_3@SiO_2@PPy (FSHP_x-*y*) were as follows: Stoichiometric FSH nanospheres were dispersed in 55 mL of aqueous solution containing pyrrole and *p*-TSA under

Table 1. Summary of reaction conditions used in the preparation of γ-Fe_2O_3@SiO_2@PPy composites.

Sample	FSH or FS (g)	Pyrrole (mmol)	pyrrole/*p*-TSA/ $FeCl_3 \cdot 6H_2O$ (molar ratio)	water solution (mL)
$FSHP_{0.6}$-1	0.6	5	1:0:4	75
$FSHP_{0.6}$-2	0.6	5	1:1:4	75
$FSHP_{0.6}$-3	0.6	5	1:2:4	75
$FSHP_{0.6}$-4	0.6	5	1:1:2	75
$FSHP_{0.05}$-2	0.05	5	1:1:4	75
$FSHP_{0.1}$-2	0.1	5	1:1:4	75
$FSHP_{0.2}$-2	0.2	5	1:1:4	75
$FSHP_{1.0}$-2	1.0	5	1:1:4	75
$FSP_{1.0}$-2	1.0	5	1:1:4	75

supersonic agitation. Under mechanical stirring at a speed of 800 rpm in an ice-water bath, 20 mL of $FeCl_3$ solution was added dropwise to the dispersion within 1 h for the in-situ oxidative polymerization of pyrrole monomers. The reaction system was kept at 0-4 °C and stirred for 6 h. Finally, the black products were collected and rinsed with deionized water and ethanol, and dried at 50 °C for 12 h.

As a reference, γ-Fe_2O_3@SiO_2@PPy nanocomposites (assigned as FSP_x-*y*) using unfunctionalized FS seeds were also prepared as a comparison to investigate the effect of -SO_3H on the morphology and conductivity of the γ-Fe_2O_3@SiO_2@PPy composites. In $FSHP_x$-*y* or FSP_x-*y*, *x* and *y* referred to the grams of FSH (or FS) and the batch number of different pyrrole/*p*-TSA/$FeCl_3$ $6H_2O$ molar ratios (Table 1), respectively.

Characterization

Field emitting scanning electron microscope (SEM, JSM-6700F), energy dispersive X-ray (EDX) and transmission electron microscope (TEM, JEM-200CX and FEI TECNAI G2 F20) were used to study the morphologies of the γ-Fe_2O_3@SiO_2-SO_3H and γ-Fe_2O_3@SiO_2@PPy nanocomposites. The thermogravimetric (TG) analysis was carried out on a SETSYS Evolution TGA (Setaram) from room temperature to 800°C at a heating rate of 10°C min^{-1} and a dynamic dry air flow. FTIR spectra (KBr pellet, Perkin-Elmer System), X-ray photoelectron spectroscopy (XPS, PHI-5702) and X-ray diffraction (XRD, RINT2000 wide angle goniometer) were used to characterize the chemical structures of the resulting nanocomposites. The magnetization curves at different magnetic field (-800 to 800 kA m^{-1}) were measured at room temperature by an extracting sample magnetometer (Lakeshore 7404). The conductivity at room temperature was measured using four-probe method with a KEITHLEY 2400 multimeter and a KEITHLEY 2182A nanovoltmeter.

Results and discussion

The whole procedure to prepare γ-Fe_2O_3@SiO_2@PPy nanospheres is illustrated in Scheme 2. First, the Fe_3O_4 NPs were prepared by chemical precipitation method and modified by citric acid to get MFs. Then, SiO_2 shell was coated on the Fe_3O_4 NPs surface through a sol–gel process. Subsequently, the achieved Fe_3O_4@SiO_2 nanospheres were transformed into γ-Fe_2O_3@SiO_2 by heating in air. After reacting MPTS with the

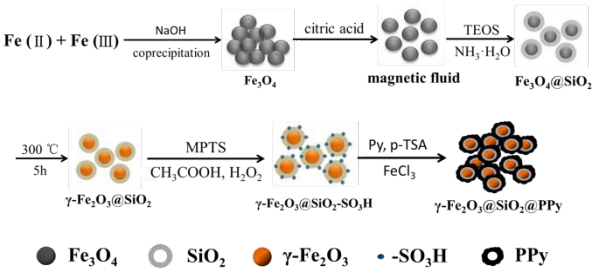

Scheme 2. A schematic diagram for the fabrication process of γ-Fe_2O_3@SiO_2@PPy nanospheres.

γ-Fe_2O_3@SiO_2 and further oxidation with H_2O_2, the –$(CH_2)_3SO_3H$ groups were successfully grafted onto SiO_2 surface. Finally, pyrrole monomer polymerized on the surface of γ-Fe_2O_3@SiO_2-SO_3H nanospheres by in situ oxidation polymerization, generating core/shell/shell γ-Fe_2O_3@SiO_2@PPy nanospheres.

Morphologies and formation mechanism

Typical SEM and TEM images of γ-Fe_2O_3@SiO_2-SO_3H, γ-Fe_2O_3@SiO_2@PPy were employed to investigate the morphologies of the as-prepared samples. SEM image (Figure 1a) indicates that the resultant γ-Fe_2O_3@SiO_2-SO_3H indeed have a nanosphere in shape, and TEM image (Figure 1a') confirms the γ-Fe_2O_3@SiO_2-SO_3H nanospheres possess a well-defined core/shell structure. Compared with γ-Fe_2O_3@SiO_2-SO_3H nanospheres, well-defined γ-Fe_2O_3@SiO_2@PPy core/shell/shell three-layer spherical structure can be observed clearly by SEM and TEM images (Figure 1b and 1b'), which indicate the polymerization of pyrrole monomers has occurred on the surface of SiO_2 shell.

It is noteworthy to mention that the surface of SiO_2 shell is hydrophilic, while pyrrole monomer is hydrophobic. In this fashion, the combination of SiO_2 with PPy is a challenge by in-situ polymerizing PPy in SiO_2 solution. We can facilely realize the homogeneous coverage of PPy on γ-Fe_2O_3@SiO_2 by anchoring PPy with modified γ-Fe_2O_3@SiO_2-SO_3H. As a reference, the unmodified γ-Fe_2O_3@SiO_2 has also been utilized as the core to prepare γ-Fe_2O_3@SiO_2@PPy nanospheres. As illustrated in TEM image of Figure 1c' the resulting γ-

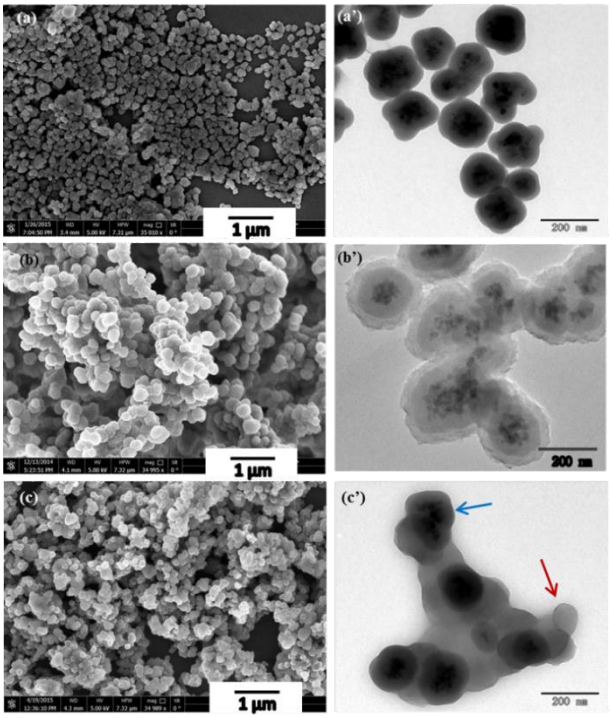

Figure 1. SEM and TEM images of FSH (a and a'); $FSHP_{1.0}$-2 (b and b'); $FSP_{1.0}$-2 (c and c'). The blue arrow represents the bare FS two-layer structure and the red arrow represents the freely deposited PPy particles.

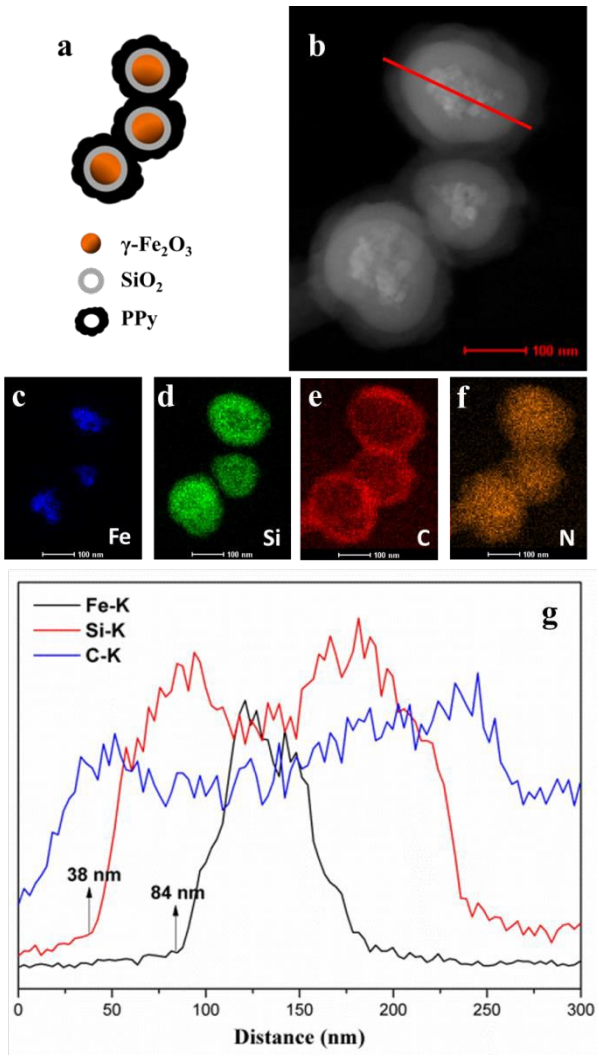

Figure 2. (a) Schematic of γ-Fe_2O_3@SiO_2@PPy nanospheres. (b) Typical HAADF STEM image of $FSHP_{1.0}$-2. (c-f) Elemental mapping of three agglutinate γ-Fe_2O_3@SiO_2@PPy nanospheres in $FSHP_{1.0}$-2 with Fe, Si, C and N signals. (g) EDS line scanning profiles of $FSHP_{1.0}$-2 across the map. The red line in (b) corresponds to the EDS line scanning region.

Fe_2O_3@SiO_2@PPy composite contains both bare γ-Fe_2O_3@SiO_2 two-layer structure (blue arrow) and freely deposited PPy particles (red arrow). In other words, the polymerization process isn't favoured on the unmodified silica surface. Therefore, -SO_3H group is the key factor to influence the core/shell/shell morphology.

Energy dispersive X-ray spectroscopy (EDX) elemental mapping of the nanospheres also clearly displays the expected core/shell/shell structure[25]. The different colour images shown in Figure 2c-f indicate Fe-, Si-, C-, and N-enriched areas of the $FSHP_{1.0}$-2 sample, respectively, which confirm the presence of both SiO_2 and PPy serving as the shell of γ-Fe_2O_3 core. The images also confirm that the coating of SiO_2 and PPy is uniform, and after the coating of PPy, the nanospheres agglutinate. The line profiles further confirm the three-layer structure (Figure2g)

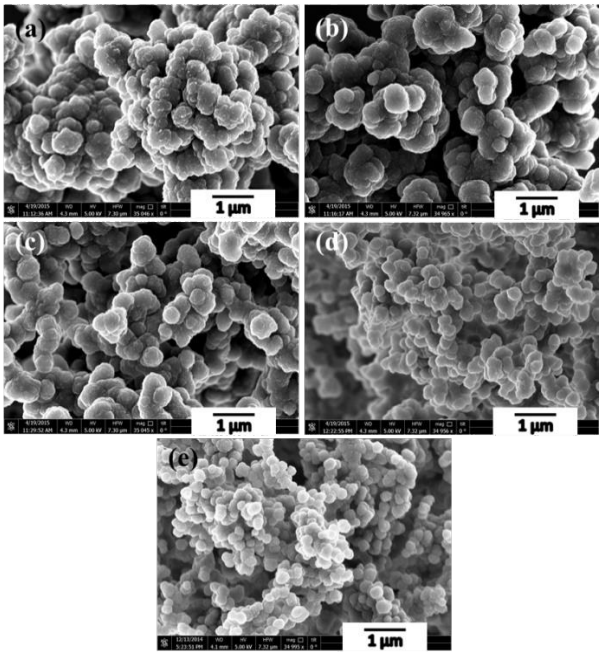

Figure 3. SEM images of (a) $FSHP_{0.05}$-2, (b) $FSHP_{0.1}$-2, (c) $FSHP_{0.2}$-2, (d) $FSHP_{0.6}$-2 and (e) $FSHP_{1.0}$-2.

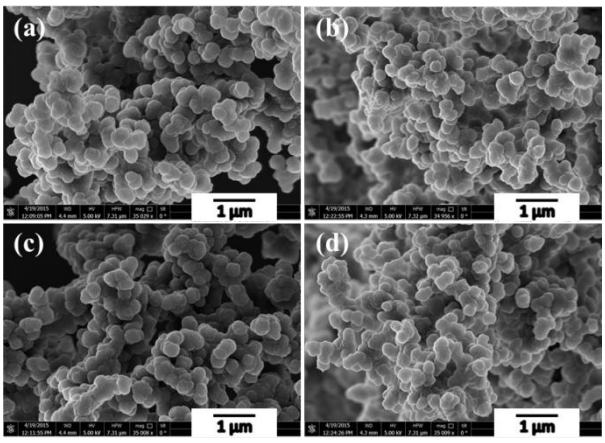

Figure 4. SEM images of (a) $FSHP_{0.6}$-1, (b) $FSHP_{0.6}$-2, (c) $FSHP_{0.6}$-3 and (d) $FSHP_{0.6}$-4.

and the 38 nm thickness of the SiO_2 shell and 46nm thickness of the PPy shell were calculated accordingly, which in correspondence with the HAADF STEM image (Figure 2b).

The synthesis conditions, as summarized in Table 1, have significant impact on the morphologies of γ-Fe_2O_3@SiO_2@PPy. Figure 3 shows the morphology evolution of γ-Fe_2O_3@SiO_2@PPy with FSH dosage ranging from 19.2 to 83.1 wt% (mass fraction calculated by TGA data, Supp. Table S1). Apparently, enhancement of FSH dosage is beneficial to homogeneous distribution of γ-Fe_2O_3@SiO_2@PPy nanospheres and to the reduction of γ-Fe_2O_3@SiO_2@PPy diameter. However, we can't find apparent deviations by tuning molar

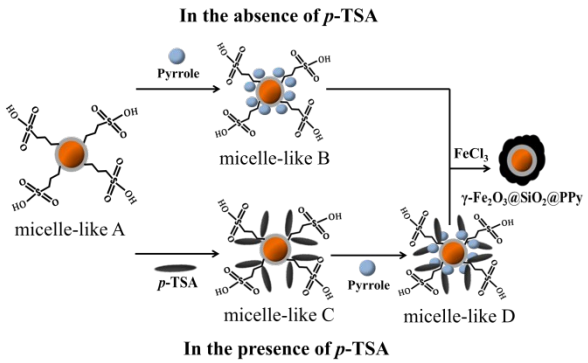

Scheme 3. Schematic illustration of the formation mechanism of the γ-Fe_2O_3@SiO_2@PPy nanospheres.

ratio of pyrrole/p-TSA/$FeCl_3$ from 1:0:4 to 1:1:2 while fixing FSH dosage of 0.6 g, yielding spherical morphology in all aspects, as shown in Figure 4. Notably, the *p*-TSA dopant does not affect the morphologies of γ-Fe_2O_3@SiO_2@PPy composites.

A possible formation mechanism behind the aforementioned results for γ-Fe_2O_3@SiO_2@PPy nanospheres is illustrated in Scheme 3. It has been widely investigated that the morphologies of PPy composites highly depend on seed templates' shape in the polymerization system of pyrrole monomers, such as particulates, nano/microspheres and nano-needles.[20,26,27] As has demonstrated in previous work,[26] the micelles consisting of *p*-TSA and pyrrole can be formed in the reaction solution resulting from the hydrophobic pyrrole adhering to the oil-wet side of *p*-TSA and the presence of hydrophilic -SO_3H group in the *p*-TSA, thus the pyrrole/*p*-TSA supermolecules serve as the "soft-templates" in the formation of PPy-*p*-TSA nanostructures. Herein, the outer –SO_3H groups are hydrophilic and the inner γ-Fe_2O_3@SiO_2-$(CH_2)_3$- structure is hydrophobic (Scheme 2), therefore the γ-Fe_2O_3@SiO_2-SO_3H nanosphere has a micelle-like structure (micelle-like A). In the absence of *p*-TSA, pristine pyrrole diffuses into the inner oil-wet side of micelle-like A to form micelle-like B. In the presence of *p*-TSA, micelle-like C occurs when the oil-wet side of *p*-TSA adheres to micelle-like A, the subsequently added pyrrole diffuses into micelle-like C to form micelle-like D. B and D are believed as the templates to form γ-Fe_2O_3@SiO_2@PPy nanospheres. Due to fact that the solubilized pyrrole molecules are oxidized by $FeCl_3$, the polymerization reaction is believed to proceed in the interface of micelles and water.[28] In our experiments, it is obvious that the micelle-like B and D mainly act as the template judged from the morphology of the as-prepared γ-Fe_2O_3@SiO_2@PPy. In case of the decided amount of pyrrole monomers and polymerization condition used in the reaction systems, the amount of the pyrrole monomers distributed to every γ-Fe_2O_3@SiO_2-SO_3H core decrease when the amount of γ-Fe_2O_3@SiO_2-SO_3H cores increase. As a result, the thickness of PPy shell decreases and thus leads to smaller diameter and more sphere-like of the γ-Fe_2O_3@SiO_2@PPy nanospheres (Figure 3a-e). On the other hand, when the amount of Fe_2O_3@SiO_2-SO_3H cores is decided, there's no apparent deviation on the morphologies (Figure 4a-d).

The typical SEM and TEM images of $FSHP_{1.0}$-2 (Figure 1b and b') show that these nanospheres are aggregated, which has also been indicated by dynamic light scattering (DLS) data (Supp. Figure S1). The mean hydrodynamic diameter of 858 nm and polydispersity (PDI) of 0.34 suggest the nanospheres are not monodispersed[29]. The aggregation of the nanospheres may result from the relatively high Hamaker constant reported for PPy[30] and the interaction between Fe^{3+} and –OH (from –SO_3H on γ-Fe_2O_3@SiO_2-SO_3H surface) in the reaction system. While some steric stabilizers such as Poly(N-vinylpyrrolidone)[31] and chitosan[20] were used in the PPy coating process, which would prevent the latex particles from aggregating, it can lead to the low and uncontrollable conductivity of the resultant composites. Herein, without the steric stabilizer, the PPy coated nanospheres have a propensity to aggregate, and on the other hand, the huge amounts of iron ions in the reaction system may lead micelle-like B or D to aggregate, and the pyrrole monomers residual in the solution are oxidized by Fe^{3+} to polymerize between the micelles, which responsible for the agglutination of the nanospheres.

Structural characterization

Figure 5 shows the thermo gravimetric analysis (TGA) curves of FS, FSH, $FSHP_{1.0}$-2 and PPy. It's reasonable to consider that the variation of residual mass fraction at 800 °C between FSH and FS is attributed to the propylsulfonic thermal degradation in FSH (Figure 5a and b). There are two obvious stages in the process of thermal decomposition for pure PPy (Figure 5d). The first stage in the range of 30-180 °C results from the evaporation of some impurities such as oligomers and absorbed water, the other one at above 330 °C is caused by the degradation of PPy chains, and it has decomposed completely above 550 °C. In contrast with the pure PPy, the temperature corresponding to maximum decomposition rate of $FSHP_{1.0}$-2 is higher than that of pure PPy, which indirectly indicates that the PPy shell indeed has some interaction with the FSH cores, thus the thermal stability of FSHP composites has been improved. The contents of magnetic FSH cores in $FSHP_x$-2 and $FSHP_{0.6}$-*y* samples have also been determined by

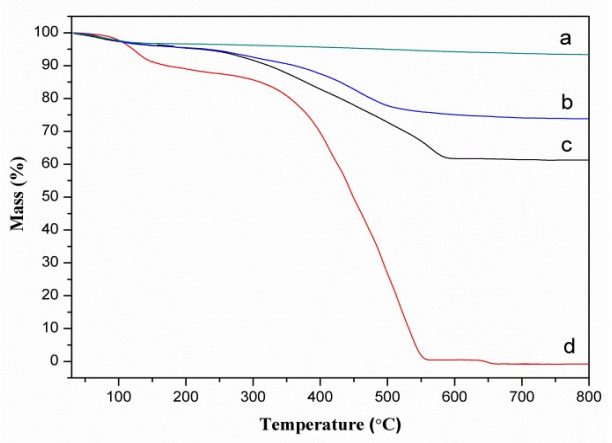

Figure 5. TG curves of FS (a), FSH (b), $FSHP_{1.0}$-2 (c), PPy (d).

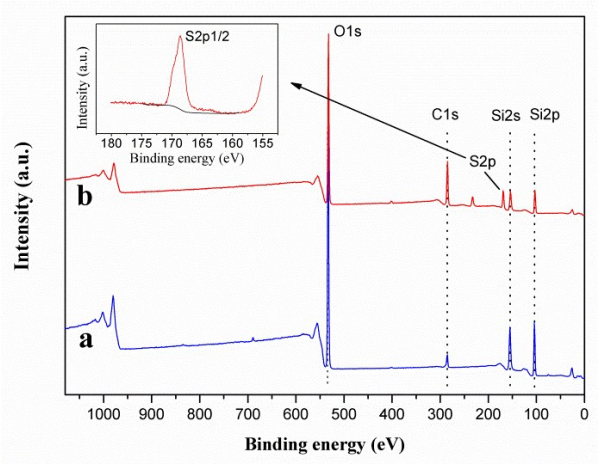

Figure 6. XPS spectra of (a) FS, (b) FSH. The inset shows the expanded spectra of S 2p.

TGA data (Supp. Figure S2, Table S1), which are responsible for the variation of magnetism of the samples.

X-photoelectron spectroscope (XPS) is utilized to determine the molecular structures. Figure 6 shows the full XPS spectrums of the as-prepared FS and FSH. In comparison with unfunctionalized FS (Figure 6a), the characteristic peak occurs at 169.1 eV is attributed to the sulfur atom from the silane coupling agent for the functionalized FSH (Figure 6b). The peak centred at 168.6 eV corresponding to -SO_3H group[32,33] is detected as shown in the S 2p high-resolution spectrum for the functionalized FSH (inset of Figure 6), while the peak near 164 eV due to the –SH group[34,35] is undetected. This result further demonstrates the mercapto groups have been oxidized completely to sulfonic ones. The S/Si atomic ratio of ~ 0.4 determined by XPS data manifests the surface of silica is enriched with sulfonic groups.[32] In addition, there is also a substantial increase in the relative intensity of C 1s peak compared with the untreated FS. The increase in the relative intensity of C 1s peak can be attributed to the propyl chain from MPTS grafted to silica. In the case of the untreated FS, the C 1s peak mainly results from adventitious carbon contamination. Besides, for both FS and FSH, the typical peaks at 155.1 and 103.5 eV are attributed to Si 2s, Si 2p, respectively, while the peaks corresponding to characteristic doublets of Fe 2p3/2 and 2p1/2 core-level spectra in iron oxide, cannot be observed. This phenomenon can be explained by the fact that the SiO_2 layer thickness (38 nm) exceeds the detecting depth of XPS measurement.

The grafting of –SO_3H groups was also confirmed by FTIR spectra. As shown in Figure 7b, FS shows the absorption bands in the range of 3654 cm^{-1} and 1260-1000 cm^{-1} assigned to Si-O-H and Si-O coordination, respectively. Other intense bands at 1635 cm^{-1} (O-H bending vibration), 966 cm^{-1} (Si-O stretching vibration), 806 cm^{-1} (Si-O-Si bending vibration) and 450 cm^{-1} (Si-O-Si rocking vibration) are also observed for FS.[19] For FSH (Figure 7c), the characteristic peaks of -SO_3H group attributed to O-H stretching vibration band centred at 3400 cm^{-1} and the

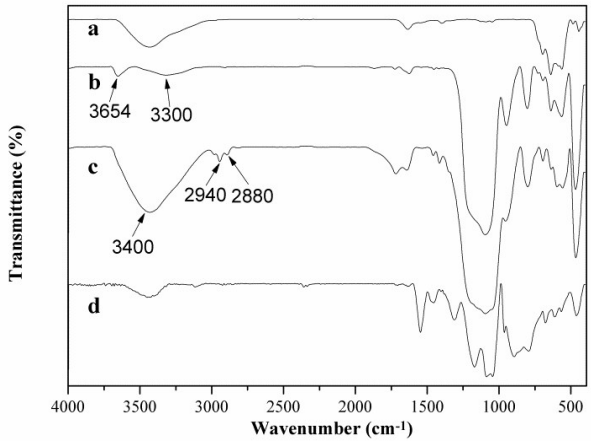

Figure 7. FTIR spectra of (a) γ-Fe_2O_3, (b) FS, (c) FSH and (d) $FSHP_{1.0}$-2.

bands at 2940, 2880 cm^{-1} (C-H stretching vibration) and 1460-1420 cm^{-1} (C-H bending vibration) related to the C-H and C-C vibrational modes of the propyl group[36] can be observed clearly. The peaks assigned to SO_2 are overlapped by the intense band of Si-O at 1260-1000 cm^{-1}. FTIR spectra indicate that the sulfonic-functionalization of γ-Fe_2O_3@SiO_2 was well done. In the FTIR spectrum of $FSHP_{1.0}$-2 (Figure 7d), the characteristic absorption bands at 1545, 1453, 1310, 1166, 1037, and 897 cm^{-1} attributed to the coated of PPy are similar to those of PPy/γ-Fe_2O_3 synthesized.[11,26] The peaks at 1545 and 1453 cm^{-1} are ascribed to the C=C and C-N stretching vibrations. The peaks at 1313 and 1186 cm^{-1} correspond to the C-H in-plane vibration. The peaks at 1037 and 885 cm^{-1} are attributed to the C-H in-plane bending and the ring deformation, respectively. These results indicate that the structure of the main PPy chain in the γ-Fe_2O_3@SiO_2@PPy nanospheres prepared is identical to those of the PPy/Fe_3O_4 nanostructures prepared previously.[37]

Figure 8 shows the XRD patterns of $FSHP_{1.0}$-2, FSH, γ-Fe_2O_3 synthesized and standard γ-Fe_2O_3. The sharp peaks at 2θ = 30.2°, 35.6°, 43.3°, 53.7°, 57.3°, and 62.9°are observed in the

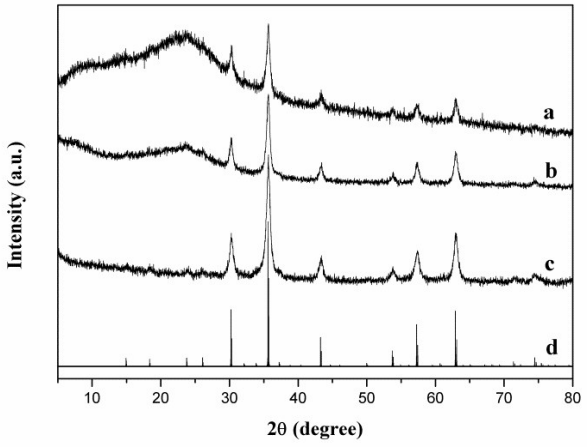

Figure 8. XRD patterns of (a) $FSHP_{1.0}$-2, (b) FSH, (c) as-synthesized γ-Fe_2O_3, and (d) standard γ-Fe_2O_3 (JCPDS No. 39-1346).

synthesized γ-Fe_2O_3 (Figure 8c), which match well with the standard peaks of γ-Fe_2O_3 (JCPDS file No. 39-1346, Figure 8d). Apart from the peaks attributed to γ-Fe_2O_3, a broad diffraction peak centred at 2θ = 23.5° attributed to the amorphous SiO_2 (Figure 8b) and a broad diffraction peak centred at 2θ = 23.5°assigned to PPy (Figure 8a) are observed in the XRD patterns of FSH and $FSHP_{1.0}$-2.[11,38]

Electrical and magnetic properties

It has been demonstrated that magnetic and electrical properties can be successfully integrated into a single COSM.[8] Subsequently, the conductivity and magnetization can be enhanced simultaneously by controlling the amounts of $FeCl_2$ ($[Fe^{II}]/[Fe^{III}]$ ratio < 0.046) for ICOSM.[9] However, the conductivity and saturation magnetization decrease negatively simultaneously when $[Fe^{II}]/[Fe^{III}]$ ratio is higher than 0.046. By controlling the synthesis conditions, as summarized in Table 1, an electrical conductivity ranging from 17 to 53 S cm^{-1} (Figure 9) and a high saturation magnetization in a range of 2.18~8.17 Am^2 kg^{-1} (Figure 10) can be realized using γ-Fe_2O_3@SiO_2-SO_3H cores. It's worth mention that the conductivities maintain a high level (50~60 S cm^{-1}) even the γ-Fe_2O_3@SiO_2-SO_3H mass fraction reaches 83.1 wt%, which can be attributed to the complete encapsulation of γ-Fe_2O_3@SiO_2-SO_3H cores by PPy shell. By contrast, the conductivity of the $FSP_{1.0}$-2 sample obtained by using unfunctionalized γ-Fe_2O_3@SiO_2 as seeds is as low as 8 S cm^{-1}, which is one magnitude lower than that of $FSHP_{1.0}$-2 (55 S cm^{-1}). Till now, we can conclude that the merits on high conductivity and high magnetization can also be integrated into a single nanosphere using the method reported here. Moreover, we can realize the independent control of electrical conductivity and saturation magnetization of the electromagnetically functionalized conducting polymer.

Figure 11 shows the dependence of magnetism (M) on applied magnetic field (H) for $FSHP_{0.6}$-*y* samples and $FSHP_x$-2 samples. All the γ-Fe_2O_3@SiO_2@PPy nanocomposites exhibit superparamagnetic behavior (i.e., no hysteretic loop). The saturation magnetization (Ms) of the γ-Fe_2O_3@SiO_2@PPy composites increases with an increase of the FSH content (Figure 11b). And when the dosage of FSH cores was decided, the obtained γ-Fe_2O_3@SiO_2@PPy composites with different polymerization conditions have slightly different contents of FSH, and the Ms of γ-Fe_2O_3@SiO_2@PPy composites is directly proportional to the contents of FSH (Figure11a).

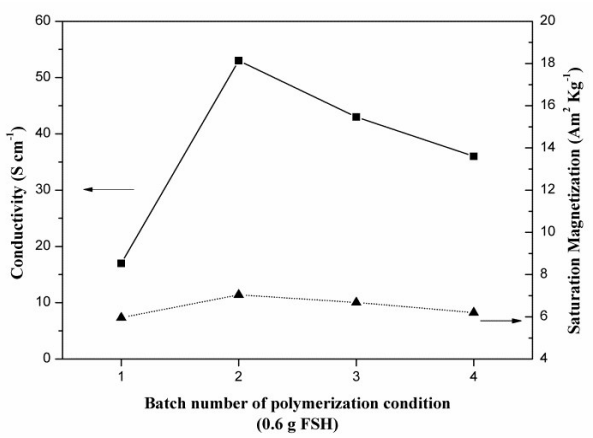

Figure 9. Effect of the polymerization condition on the conductivity and saturation magnetization of $FSHP_{0.6}$-γ samples.

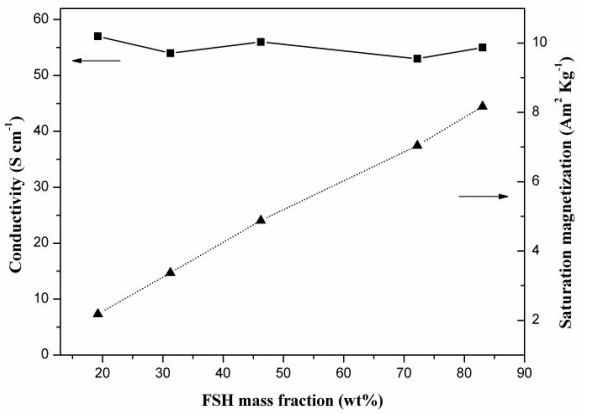

Figure 10. Effect of the FSH mass fraction on the conductivity and saturation magnetization of $FSHP_x$-2 samples.

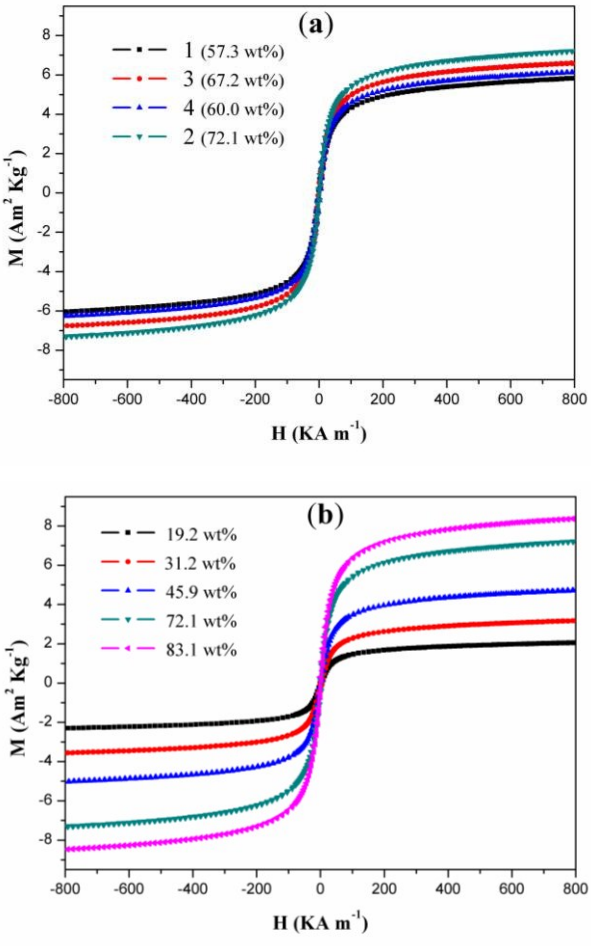

Figure 11. Dependence of the magnetism on the applied magnetic field at room temperature: (a) $FSHP_{0.6}$-γ samples with different polymerization conditions; (b) $FSHP_x$-2 samples with different FSH dosages. FSH mass fractions were given based on TGA data.

Conclusions

Electromagnetic functionalized γ-Fe_2O_3@SiO_2@PPy core/shell/shell nanospheres have been successfully realized by in-situ polymerization of pyrrole monomers in the presence of spherical γ-Fe_2O_3@SiO_2-SO_3H templates. A prerequisite of realizing the γ-Fe_2O_3@SiO_2@PPy nanospheres is to anchor PPy shell onto SiO_2 surface by -SO_3H groups, allowing for the homogeneously spherical morphology and high conductivity of the γ-Fe_2O_3@SiO_2@PPy composites at high γ-Fe_2O_3@SiO_2-SO_3H dosage. In particularly, the conductivity as high as 17~53 S cm^{-1} and saturation magnetization of 2.18~8.17 Am^2 kg^{-1} can be independently tuned by controlling polymerization conditions and γ-Fe_2O_3@SiO_2-SO_3H dosages.

Acknowledgements

This project was supported by the National Natural Science Foundation of China (No.41476059) and National Science and Technology Support Program (2012BAB15B02).

References

1 B. Zhang, Y. Du, P. Zhang, H. Zhao, L. Kang, X. Han and P. Xu, *J. Appl. Polym. Sci.*, 2013, **130**, 1909−1916.

2 F. Xu, L. Ma, Q. Huo, M. Gan and J. Tang, *J. Magn. Magn. Mater.*, 2015, **374**, 311−316.

3 C. Cui, Y. Du, T. Li, X. Zheng, X. Wang, X. Han and P. J. Xu, *J. Phys. Chem. B*, 2012, **116**, 9523−9531.

4 Y. F. Zhu, Q. Q. Ni, Y. Q. Fu and T. Natsuki, *J. Nanopart. Res.*, 2013, **15**, 1988−1998.

5 O. Akman, Z. Durmus, H. Kavas, B. Aktas, U. Kurtan, A. Baykal and H. Sözeri, *Phys. Status Solidi A*, 2013, **210**, 395−402.

6 Z. Zhang and M. Wan, *Synth. Met.*, 2003, **132**, 205−212.

7 Z. Zhang, M. Wan and Y. Wei, *Nanotechnology*, 2005, **16**, 2827−2832.

8 Z. Zhang, J. Deng, J. Shen, M. Wan, and Z. Chen, *Macromol. Rapid Commun.*, 2007, **28**, 585−590.

9 Z. Zhang, Q. Li, L. Yu, Z. Cui, L. Zhang and G. A. Bowmaker, *Macromolecules*, 2011, **44**, 4610−4615.

10 J. W. Liu, R. C. Che, H. J. Chen, F. Zhang, F. Xia, Q. S. Wu and M. Wang, *Small*, 2012, **8**, 1214−1221.

11 Y. J. Chen, F. Zhang, G. G. Zhao, X. Y. Fang, H. B. Jin, P. Gao, C. L. Zhu, M. S. Cao and G. Xiao, *J. Phys. Chem. C*, 2010, **114**, 9239−9244.

12 G. Wang, Y. Chang, L. Wang and C. Liu, *Adv. Powder Technol.*, 2012, **23**, 861−865.

13 W. C. Zhou, X. J. Hu, X. X. Bai, S. Y. Zhou, C. H. Sun, J. Yan and P. Chen, *ACS Appl. Mater. Int.*, 2011, **3**, 3839−3845.

14 Y. H. Deng, C. C. Wang, J. H. Hu, W. L. Yang and S. K. Fu, *Colloids Surf., A: Physicochem. Eng. Aspects*, 2005, **262**, 87−93.

15 M. Chehimi, M. M. Chehimi, D. Mordenti, M. Bri and M. Delamará, *J. Mater. Chem.*, 1998, **8**, 2185−2193.

16 C. Perruchot, M. M. Chehimi, M. Delamar and F. Fievet, *Surf. Interface Anal.*, 1998, **26**, 689−698.

17 T. Dai, X. Yang and Y. Lu, *Mater. Lett.*, 2007, **61**, 3142−3145.

18 C. H. Tang, M.S. Thesis, Beijing University of Chemical Technology, China, 2011.

19 L. C. Fonseca, R. Faez, F. F. Camilo and M. A. Bizeto, *Microporous Mesoporous Mater.*, 2012, **159**, 24−29.

20 X. Yang, T. Dai and Y. Lu, *Polymer*, 2006, **47**, 441−447.

21 L. Hao, C. Zhu, C. Chen, P. Kang, Y. Hu, W. Fan and Z. Chen, *Synth. Met.*, 2003, **139**, 391−396.

22 J. H. Zhu, S. Y. Wei, N. Haldolaarachchige, D. P. Young and Z. H. Guo, *J. Phys. Chem. C*, 2011, **115**, 15304–15310.

23 Y. Yang, Z. W. Li, C. P. Neo and J. Ding, *J. Phys. Chem. Solids*, 2014, **75**, 230-235.

24 B. Liu, D. P. Wang and W. H. Huang, *J. Funct. Mater.*, (in Chinese) 2007, **38**, 1074−1077.

25 P. C. Naha, A. A. Zaki, E. Hecht, M. Chorny, P. Chhour, E. Blankemeyer, D. M. Yates, W. R. Witschey, H. I. Litt, A. Tsourkas and D. P. Cormode, *J. Mater. Chem. B, Mater. Biol. Med.*, 2014, **2**, 8239–8248.

26 H. M. Xiao, W. D. Zhang, M. X. Wan and S. Y. Fu, *J. Polym. Sci., Part A: Polym. Chem.*, 2009, **47**, 4446−4453.

27 X. Li, M. Wan, Y. Wei, J. Shen and Z. Chen, *J. Phys. Chem. B*, 2006, **110**, 14623−14626.

28 B. J. Kim, S. G. Oh, M. G. Han and S. S. Im, *Synth. Met.*, 2001, **122**, 297−304.

29 A. L. Brown, P. C. Naha, V. Benavides-Montes, H. I. Litt, A. M. Goforth and D. P. Cormode, *Chem. Mater.*, 2014, **26**, 2266-2274.

30 M. M. Chehimi, S. F. Lascelles and S. P. Armes, *Chromatographia*, 1995, **41**, 671−677.

31 C. Mangeney, M. Fertani, S. Bousalem, M. Zhicai, S. Ammar, F. Herbst, P. Beaunier, A. Elaissari and M. M. Chehimi, *Langmuir*, 2007, **23**, 10940-10949.

32 M. D. González, P. Salagre, E. Taboada, J. Llorca, E. Molins and Y. Cesteros, *Appl. Catal., B: Environ.*, 2013, **136**, 287−293.

33 M. M. Nasef and H. Saidi, *Appl. Surf. Sci.*, 2006, **252**, 3073−3084.

34 Z. C. Liu, Q. G. He, P. Hou, P. F. Xiao, N. Y. He and Z. H. Lu, *Colloids Surf., A: Physicochem. Eng. Aspects*, 2005, **257**, 283−286.

35 R. Lenigk, M. Carles, N. Y. Ip and N. J. Sucher, *Langmuir*, 2001, **17**, 2497-2501.

36 Q. Qu, Q. Gu, Z. Gu, Y. Shen, C. Wang and X. Hu, *Colloids Surf., A: Physicochem. Eng. Aspects*, 2012, **415**, 41−46.

37 W. D. Zhang, H. M. Xiao, L. P. Zhu, S. Y. Fu and M. X. Wan, *J. Polym. Sci., Part A: Polym. Chem.*, 2010, **48**, 320−326.

38 F. Lv, L. Fu, E. P. Giannelis and G. Qi, *Solid State Sci.*, 2014, **34**, 49-55.

Table of contents

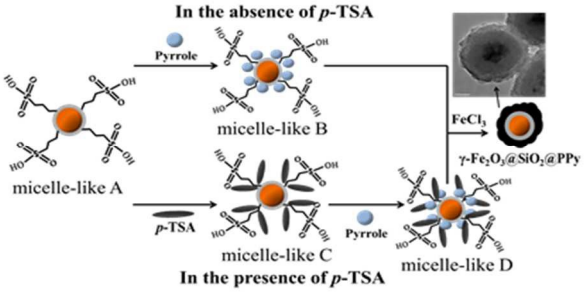

A possible formation mechanism for γ-Fe_2O_3@SiO_2@PPy core/shell/shell nanospheres with flexible controllability of electromagnetic properties is proposed.